Integrated circuit ceramic ball grid array package antenna

Zhang, Yue Ping

2004

Zhang, Y. P. (2004). Integrated circuit ceramic ball grid array package antenna. IEEE Transactions On Antennas And Propagation. 52(10), 2538-2544.

https://hdl.handle.net/10356/91243

https://doi.org/10.1109/TAP.2004.834427

Integrated Circuit Ceramic Ball Grid Array Package Antenna

Y. P. Zhang

***Abstract*—The recent advances in such highly integrated RF transceivers as radio system-on-chip and radio system-in-package have called for the parallel development of compact and efficient antennas. This paper addresses the development of a new type of dielectric chip antenna known as integrated circuit package antenna (ICPA) for highly integrated RF transceivers. A compact ICPA of this type has, for the first time, been designed and fabricated in a ceramic ball grid array (CBGA) package format. The novel ICPA, except economical advantage of mass production and automatic assembly, has potential benefit to the system-level board miniaturization and the system-level manufacturing facilitation. The simulated and measured antenna performance of the ICPA is presented. The effects of the different physical parts of the ICPA on the antenna performance are investigated. Results show that the ICPA achieved impedance bandwidth of 4.1% and radiation efficiency of 72%, and gain of 4.8 dBi at 5.715 GHz.**

***Index Terms*—Ceramic ball grid array (CBGA) package, chip antennas, radio system-in-package (SiP), radio system-on-chip (SoC).**

I. Introduction

MOTIVATED by huge demand for low-cost low-power personal wireless communications systems, many semiconductor companies have focused their attention to the development of highly integrated RF transceivers. Significant advances have been achieved in highly integrated RF transceivers through the use of advanced component integration processes and advanced component packaging technologies. For example, the single-chip and single-package radios have been demonstrated recently for Bluetooth and HIPERLAN applications. In the single-chip radios, the zero- or low-IF architectures are utilized and all components are integrated on a single silicon chip in submicron CMOS technology [1], [2]; while in the single-package radios, the heterodyne or super-heterodyne architectures are employed and several bare chips optimized in different semiconductor technologies are squeezed into a single package [3], [4].

To suit these novel solutions of highly integrated wireless transceivers, a number of dielectric chip antennas have been developed in the past few years as the result of a great effort involving the development of new dielectric materials [5], [6], the application of novel fabrication technologies [7], [8], and the optimization of various radiator structures [9], [10]. These dielectric chip antennas are physically small, they are, however, still discrete. Hence, designs of antennas on multilayer substrates in which RFICs can be embedded have been proposed [11], [12]. In this paper, the development of a new type of dielectric chip antenna known as integrated circuit package antenna (ICPA) is reported. A compact ICPA of this type has, for the first time, been designed and fabricated in a ceramic ball grid array (CBGA) package format. The configuration, the FDTD simulation, and the experimental validation of the ICPA are presented in Section II. The effects of the different physical parts of the ICPA on the antenna performance are investigated in Section III. Finally, Section IV summarizes the conclusions.

Manuscript received May 21, 2002; revised January 12, 2004

The author is with the School of Electrical and Electronic Engineering, Nanyang Technological University, Singapore 639798, Singapore (e-mail: eypzhang@ntu.edu.sg).

Digital Object Identifier 10.1109/TAP.2004.834427

II. Design of ICPA

CBGA packages have been widely used to carry highly integrated RF transceivers because of their excellent performance [3], [13]. Fig. 1(a) shows the configuration of the ICPA in a CBGA package format. As shown, the ICPA consists of three laminated ceramic layers with a cavity formed in the middle. There are two metallic layers in the construction. The bottom metallic layer provides the metallization for the cavity base and the signal traces, while the upper metallic layer provides the metallization for the radiator. It should be noted that only two of the three laminated ceramic layers are used as the effective substrate of the ICPA, which is different from the design of conventional multilayer antennas where all layers are used as the substrates of the antennas [11], [12]. The ICPA has the dimensions of 17 mm $\times$ 17 mm $\times$ 2 mm. The package ceramic material is alumina with dielectric constant of 9.7 and the package metallic material is copper with conductivity of 3.7×10^7 S/m. Fig. 1(b) shows the geometry of the radiator layer. It is seen that the radiator takes the basic form of a microstrip patch on a substrate of the high permittivity $\varepsilon_r = 9.7$. Actually, the radiator may take any other form of a printed circuit antenna structure such as a meander-line or a stacked-patch to meet the design requirement [9], [11]. The microstrip patch has the size of 14 mm $\times$ 11 mm. The middle layer has a cavity of dimensions 13 mm $\times$ 13 mm $\times$ 0.67 mm. Fig. 1(c) shows the details of the bottom layer. As shown, there are 48 signal traces. These 48 signal traces follow the current designs of highly integrated RF transceivers where 48 I/O pads are often adopted [3], [14]. It is believed that the number of I/O pads will decrease as the level of integration of RF transceivers increases. The outer ends of all 48 signal traces are connected to 48 solder balls through 48 vias, while the inner ends of 45 signal traces will be connected to the bare single-chip radio or the naked single-package radio through 45 bond wires if the ICPA is used to carry the highly integrated RF transceiver. There are 3 signal traces directly linked to the cavity base. The cavity base is also the ICPA ground plane. This shared ground is more reliable than that of the via-array realized grounds [11], [12]. The ICPA was fabricated with the

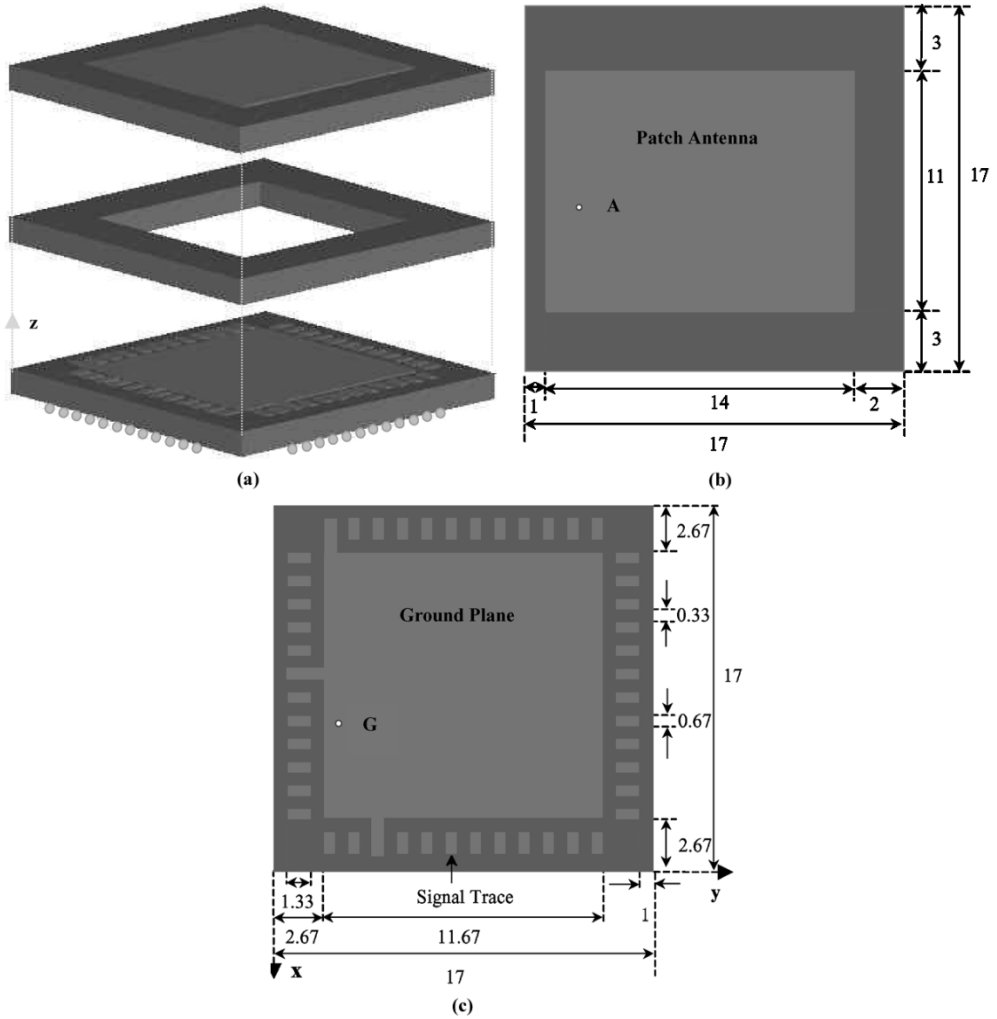

Fig. 1. Integrated ceramic ball grid array package antenna (ICPA): (a) multilayer structure, (b) radiator layer, and (c) bottom layer.

in-house facility. The fabrication of the ICPA was found to be compatible to the fabrication of the standard CBGA package. The ICPA advantage is quite obvious. It offers the possibility to combine a dielectric chip antenna with a highly integrated RF transceiver into a standard surface mounted device [15], [16]. As a result, the system-level board space and the system-level manufacturing can be further reduced and facilitated, respectively.

The development of the ICPA is quite challenging because it involves the codesign of the antenna and package. The codesign requires a versatile numerical tool that can simulate both metallic and dielectric structures. The FDTD method was chosen because of its applicability to such problems [17]–[19]. To model the ICPA, the spatial step sizes $\Delta x, \Delta y$, and Δz have to be properly chosen so that an integral number of Yee cells can fit the ICPA. Furthermore, the spatial step sizes should be much less than the smallest guided wavelength λ_{g} for accuracy. In our simulations the spatial step sizes were chosen to be $\Delta x = \Delta y = \Delta z = 0.333$ mm. Thus, the ICPA was fitted with $51 \times 51 \times 6$ cells and also the spatial step sizes were much smaller than the smallest guided wavelength $\lambda_{\mathrm{g}} = \mathrm{from}\ 16.1\ \mathrm{to}\ 19.3$ mm, which corresponds to free space wavelength $\lambda_{\mathrm{o}} = \mathrm{from}\ 50\ \mathrm{to}\ 60$ mm in C band. A via was three spatial step sizes long. A signal path was three spatial step sizes long and two spatial step size wide. A solder ball was approximately represented by $2 \times 2 \times 1$ cells. To calculate the far-field patterns, the additional free space mesh cells were added in all six sides of the ICPA. The total computational space was $85 \times 85 \times 45$ cells. The outer boundary was second order stabilized Liao [20]. In our simulation the radiator was fed through a via of four spatial step sizes long. The via was located between points G and A as marked in Fig. 1(b) and (c). A gap of length Δz was realized along the via. The lower end of the gap is at the ground point G. A Gaussian pulse was inserted in the gap to energize the ICPA. The time step in our simulations was $\Delta t = 614.3$ fs, which satisfies the Courant stability criterion. The Gaussian pulse width was 32 time steps. The source resistance was set to 50 Ω to reduce the time steps needed for FDTD calculations. It was found that 10 000 time steps were sufficient for our simulations. In our measurement the radiator was fed with the probe of an SMA connector. The probe was soldered at point A on the ICPA radiator though a small cut at point G on the ICPA ground plane. The ICPA ground plane were soldered together with the probe ground. The measurement was conducted with an HP 8510C network analyzer inside the NTU compact range.

Fig. 2 shows the simulated impedance characteristics of the ICPA. The impedance characteristics give insight on how the ICPA must be modified to achieve a specified resonant

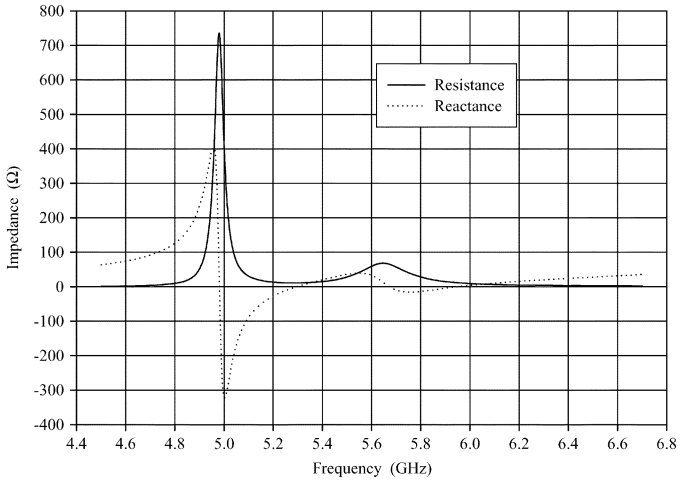

Fig. 2. ICPA input impedance versus frequency.

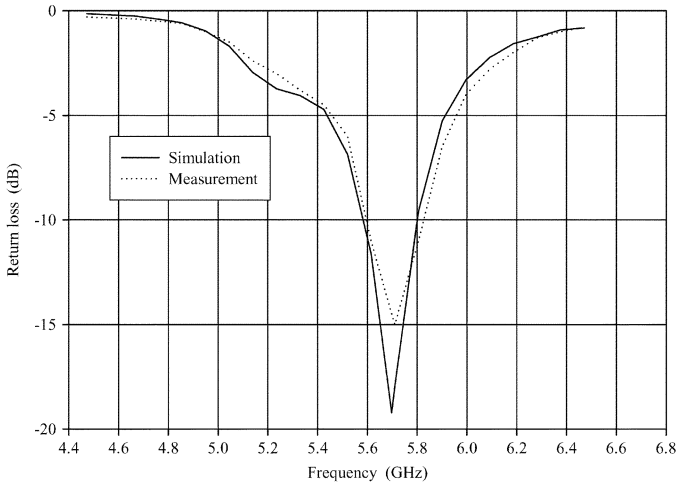

Fig. 3. ICPA return loss versus frequency.

frequency. Here the resonant frequency is defined as where the reactance of the input impedance is equal to zero. According to this definition, there are four resonant frequencies for the ICPA over the frequency range of interest from 4.5 to 6.5 GHz. At the first or lowest resonant frequency, the resistance is quite large, while at the second and the fourth or highest resonant frequencies the resistance are quite small. It is only at the third resonant frequency that the resistance is close to 50 Ω. This is expected as the third resonant frequency is the frequency at which the ICPA was designed to operate. It is evident that the impedance characteristics at the frequency of operation exhibit a small peak in the resistance and a gentle swing in the reactance from inductive to capacitive.

Fig. 3 compares the simulated and measured return loss of the ICPA. The return loss indicates how well the ICPA is matched to a signal source and how wide the impedance bandwidth is. The impedance bandwidth is the difference between the upper and lower frequencies for which the return loss is less than or equal to -10 dB. The percentage bandwidth is defined here as the difference between the upper and lower frequencies for which the return loss is less than or equal to -10 dB divided by the average of the upper and lower frequencies. It is seen that the simulated return loss agree well with measurements. The return

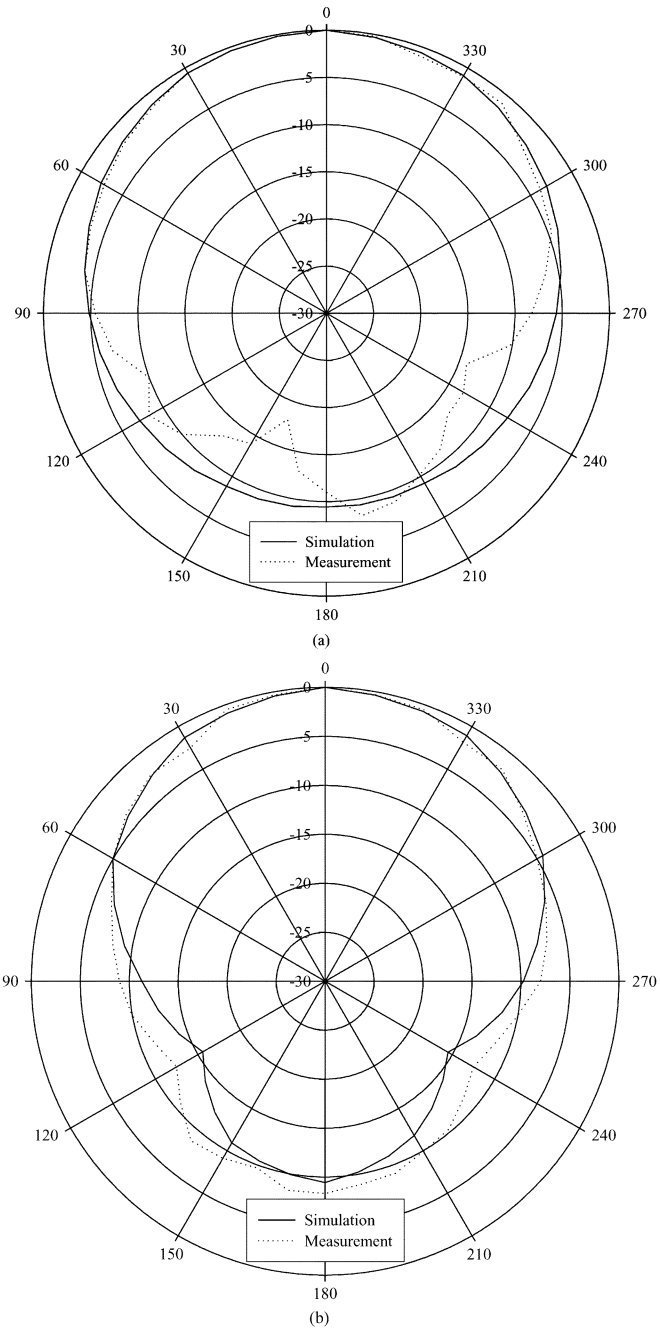

Fig. 4. ICPA radiation patterns: (a) in the E-plane and (b) in the H-plane.

loss below -10 dB at the frequency of operation indicates acceptable matching between the ICPA and the 50-Ω signal source is achieved. The simulated and measured impedance bandwidth of the ICPA are 200 MHz $(200/5695 = 3.5\%)$ and 235 MHz $(235/5715 = 4.1\%)$, respectively. A slightly wider measured impedance bandwidth may be caused by a slightly bigger cavity size due to the fabrication tolerance.

Fig. 4 illustrates the simulated and measured radiation patterns of the ICPA. It can be observed that good agreement for the upper half plane is obtained. Due to the interaction between the radiation from the ICPA and the feeding cable, the measured radiation patterns show fluctuations particularly in the E-plane, as a result, poor agreement occurs in the lower half plane. The

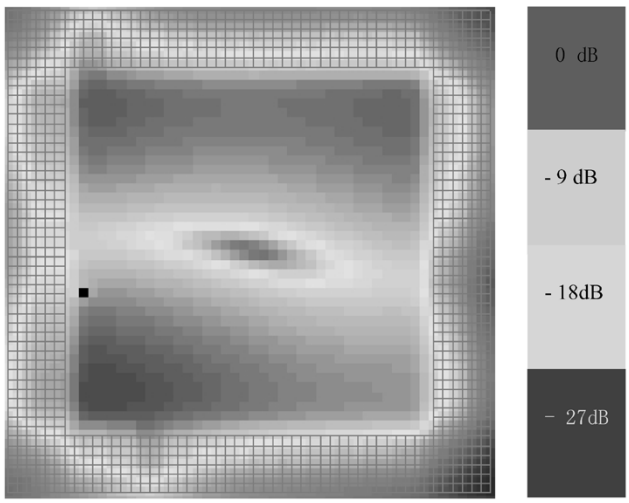

Fig. 5. Calculated electric field E_z on the cavity middle plane at the third resonant frequency 5.673 GHz.

radiation is stronger in the upper hemisphere, i.e., in the direction normal to the ICPA. This feature of the radiation patterns is desirable because it not only helps improve the efficiency of the ICPA but also reduces the interaction of the ICPA with the human body. The efficiency of the ICPA was calculated to be 72%. In addition, it should be mentioned that the ICPA has much shorter distance to the RF output of the wireless transceiver than a conventional dielectric chip antenna; this implies a smaller transmission loss, which can be translated as an improvement to the ICPA efficiency by a few percent. The gain of the ICPA was found to be 4.8 dBi, which is almost 4 dB higher than gain of most conventional dielectric chip antennas.

Fig. 5 shows the electric field component on the cavity middle plane perpendicular to the ICPA at the resonant frequency 5.673 GHz. The plot provides useful information on the location of the highly integrated RF transceiver. Due to the unsymmetrical pattern of the signal traces the electric field distribution lacks symmetry. Novertheless, the electric field reaches the minimum in the middle of the cavity and the maximum at the edges of the cavity. Thus the highly integrated RF transceiver should be located in the middle of the cavity to reduce the potential undesirable effect between the antenna and the transceiver. The detrimental effect of the power leakage of the antenna on the carried transceiver can be further reduced through shielding techniques. Depending on the semiconductor technology used for the carried transceiver, the shielding techniques can be simple or sophisticated. For instance, if the carried transceiver is in CMOS that has better linearity, an additional ground plane inserting between the antenna patch and the cavity ceiling should be sufficient [15]. However, if the carried transceiver is in Bipolar, the sophisticated shielding technique developed in [16] can be used.

III. Characterization of ICPA on CBGA Package

With reference to the ICPA studied above, an extensive series of simulations were conducted to investigate how the different physical parts of the ICPA affect the antenna performance. The simulations transformed to the frequency domain had a high resolution of 1.4 MHz. The removal of solder balls was first considered and the ICPA was thus in a ceramic pin grid array (CPGA) package format. The reduction of signal traces to 24 was then followed. It is known that the future highly integrated RF transceivers will not need many signal traces together with the associated vias and balls. Next, the variation of the cavity size was simulated. The cavity size must be large enough to accommodate a bare single-chip or a naked single-package radio. Currently, the typical size of the bare single-chip and the naked single-package radios are approximately 4 mm $\times$ 4 mm and 7 mm $\times$ 7 mm, respectively. It is predicted that their size will increase as more functions need to be integrated. Finally, the adjustment of the thickness of the top and bottom layers was modeled while the thickness of the whole ICPA and the middle layer remained unchanged. The thinner top layer allows passive components such as decoupling capacitors to be embedded in the thicker bottom layer, while the thinner bottom layer allows a bandpass filter or even a bulun to be built in the thicker top layer. The results obtained from these simulations are discussed below. It is hoped that these results can be used to develop a design methodology for integrated circuit package antennas.

Fig. 6 shows the input impedance characteristics with respect to various alterations to the ICPA. The input impedance at the third resonant frequency is scrutinized. Note that the resonant frequency increases, so does the resonant resistance when the solder balls are removed or the signal traces are reduced. The increase in the resonant frequency from 5.673 GHz to 5.75 GHz and further to 5.78 GHz and in the resistance from 65 Ω to 68 and further to 71 Ω are because the removal of solder balls or the reduction of signal traces lowers the equivalent capacitance and conductivity of the whole ICPA. Also note that the resonant frequency moves up to 5.757 GHz and the resonant resistance drops to 53 Ω when the cavity size gets bigger 13.33 mm $\times$ 13.33 mm $\times$ 0.67 mm and the resonant frequency moves down to 5.62 GHz and the resonant resistance rises to 74 Ω when the cavity size gets smaller 12.65 mm $\times$ 12.65 mm $\times$ 0.67 mm. The dependance of the input impedance on the cavity size can be attributed to the change of the cavity size that modifies the effective permittivity of the substrate of the ICPA. It is known that the resonant frequency of a microstrip patch antenna is inversely proportional to the square root of the effective permittivity of the substrate of the microstrip patch antenna and the resonant resistance of a microstrip patch antenna generally increases as the effective permittivity of the substrate of the microstrip antenna increases [21]. For the ICPA, a bigger cavity size results in a smaller effective permittivity of the substrate of the ICPA, so the resonant frequency increases and the resonant resistance decreases; while a smaller cavity size yields a bigger effective permittivity of the substrate of the ICPA, as a result, the resonant frequency decreases and the resonant resistance increases. Finally, it is interesting to note that the input impedance are affected significantly when the physical thickness of the top and bottom layers are adjusted. The resonant frequency increases to 6.31 GHz and the resonant resistance decreases to 34 Ω when the top and bottom layers become thin and thick by 0.333 mm, respectively. On the other hand, the resonant frequency decreases to 5.32 GHz and the resonant resistance increase to 104 Ω when the top and bottom layers become thick and thin by 0.333 mm, respectively. The dependance of the input impedance on the

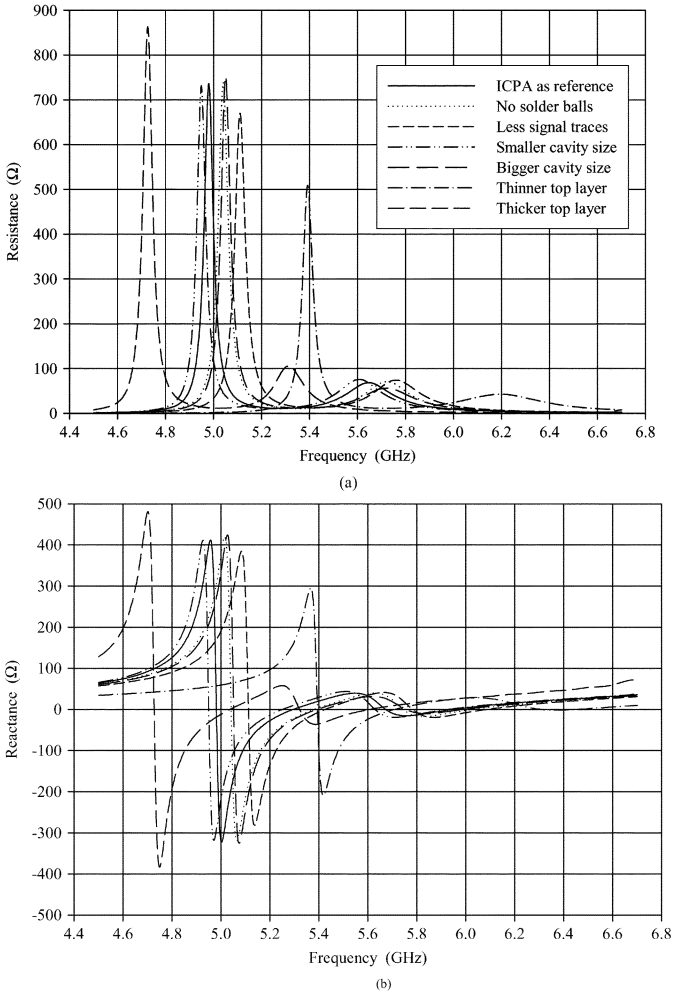

Fig. 6. Impedance versus frequency for various alterations to ICPA.

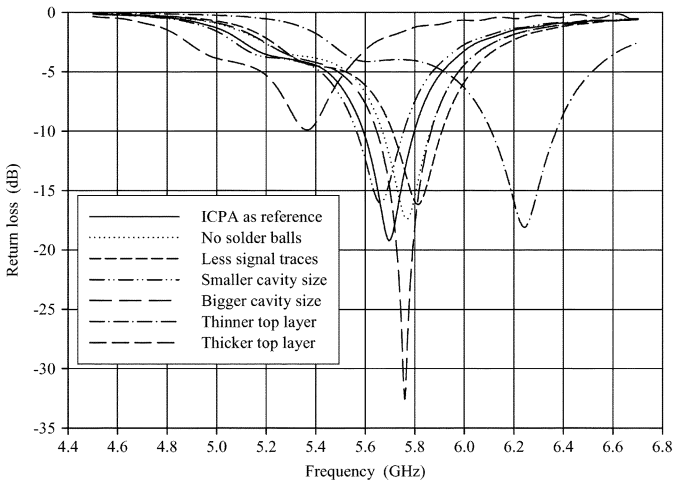

Fig. 7. Return loss versus frequency for various alterations to ICPA.

thickness of the top and bottom layers can be explained as follows. The adjustment of the physical thickness of the top and bottom layers changes the electrical thickness of the substrate of the ICPA. The electrical thickness of the substrate of the ICPA reduces to 0.019 for the case of the thinner top (0.333 mm) and thicker bottom (0.999 mm) layers and increases to 0.031 for the case of the thicker top (0.999 mm) and thinner bottom (0.333 mm) layers, respectively. Also, the adjustment of the physical thickness of the top and bottom layers changes the effective permittivity of the substrate of the ICPA. The effective permittivity of the substrate of the ICPA decreases for the case of the thinner top and thicker bottom layers and increases for the case of the thicker top and thinner bottom layers [22]. Both reduced electrical thickness and effective permittivity of the substrate of the ICPA make the resonant frequency of the ICPA increase and the resonant resistance of the ICPA decrease for the case of the thinner top and thicker bottom layers; while both increased electrical thickness and effective permittivity of the substrate of the ICPA make the resonant frequency of the ICPA decrease and the resonant resistance of the ICPA increase for the case of the thicker top and thinner bottom layers [21], [22].

Fig. 7 shows the return loss with respect to various alterations to the ICPA. Note the return loss become deteriorated for most cases. Only for the case of the bigger cavity size is the return loss improved. This is because the resonant resistance is either too larger than or much smaller than the source impedance of 50 Ω for most cases, while it is 53 Ω for the case of the bigger cavity size that is quite close to the source impedance of 50 Ω. Moreover, the impedance bandwidth are affected by these modifications. The impedance bandwidth get slightly narrower 191 MHz $(191/5660 = 3.4\%)$, 193 MHz $(193/5766 = 3.4\%)$, and 198 MHz $(198/5800 = 3.4\%)$ for the cases of the smaller cavity size, removal of solder balls, and reduction of signal traces, respectively. The smaller cavity size makes the effective permittivity of the substrate of the ICPA a slightly bigger and so the impedance bandwidth a slightly narrower. The removal of solder balls or the reduction of signal traces somewhat decrease slightly the conductor loss, in other word, increases slightly the quality factor of the ICPA, hence, causes the impedance bandwidth to be slightly narrower. The impedance bandwidth become wider for the cases of the bigger cavity size 219 MHz $(219/5757 = 3.8\%)$ and the thinner top layer 270 MHz $(270/6235 = 4.3\%)$, respectively. It is clear that the wider impedance bandwidth for the bigger cavity size is the result of the smaller effective permittivity of the substrate of the ICPA. However, it was not expected that the impedance bandwidth is wider for the case of the thinner top and thicker bottom layers. It is known that for this case both electrical thickness and effective permittivity of the substrate of the ICPA are reduced. The thinner electrical thickness reduces the impedance bandwidth but the lower permittivity enhances the impedance bandwidth much more effectively. The net effect results in the wider impedance bandwidth for the case [22]. The impedance bandwidth for the case of the thicker top and thinner bottom layers cannot be obtained because the return loss is above -10 dB. However, it is worthwhile pointing out that the thicker top layer is beneficial to the impedance bandwidth, while the resultant higher effective permittivity will narrow the impedance bandwidth.

Fig. 8 shows the radiation patterns with respect to various alterations to the ICPA. The radiation patterns do not change their shapes significantly for the cases of the removal of the solder balls, the reduction of the signal traces, and the variation of the cavity size. This is because these alterations do not significantly change the resonant frequency of the ICPA and the electromagnetic field distribution under the microstrip patch. The fundamental electromagnetic mode E_{10} generates the

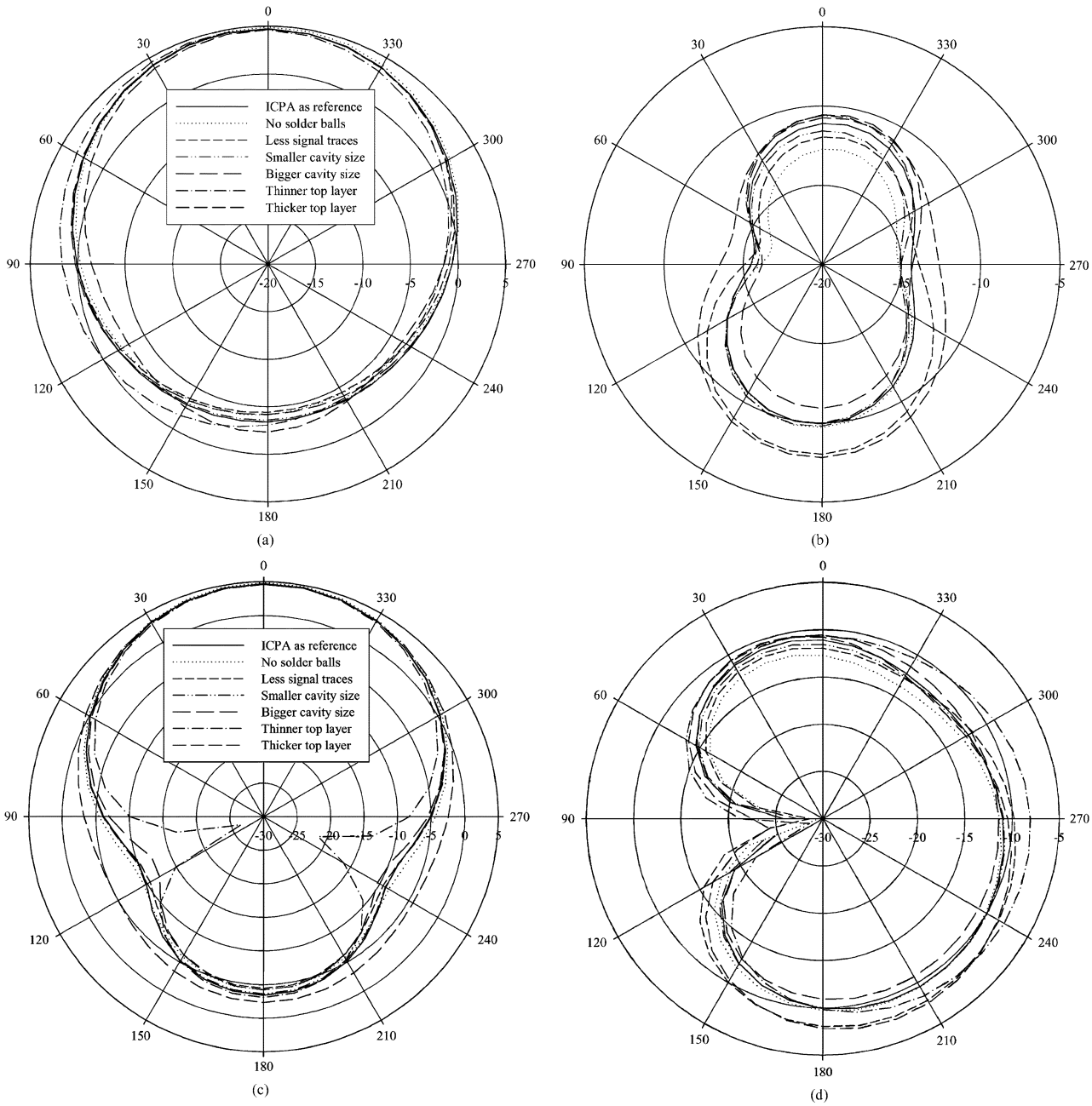

Fig. 8. ICPA radiation patterns with respect to various alterations: (a) co-polarization in the E-plane, (b) cross-polarization in the E-plane, (c) co-polarization in the H-plane, and (d) cross-polarization in the H-plane.

co-polarization radiation, while the higher mode E_{20} generates the cross-polarization radiation. The other modes contribute to either co- or cross-polarization radiation with less significant effect. The radiation patterns, however, change their shapes noticeably for the case of the adjustment of the thickness of the top and bottom layers. This is expected as the adjustment considerably affects the resonant frequency of the ICPA. For the ICPA with the thinner top and thicker bottom layers, the resonant frequency becomes higher, which makes the ground plane appear relatively larger, so the nulls in the backlobe in the co-polarization H-plane go deeper. Similarly, the ground plane appears relatively smaller for the ICPA with the thicker top and thinner bottom layers, thus the nulls in the backlobe in the co-polarization H-plane become shallower. Nevertheless, except the small asymmetry, the radiation patterns of the ICPA are similar to those of a conventional microstrip antenna on a small ground plane, that is, the radiation is stronger in the upper hemisphere. The small asymmetry in the radiation patterns is mainly caused by the grounded traces. They are linked asymmetrically to the ICPA ground plane and make the electric field distribution under the patch lack symmetry; as a result, the radiation patterns exhibit the small asymmetry. The small asymmetry in the radiation patterns disappears when the grounded traces become the signal traces like others. In other words, the radiation patterns become symmetrical when the pattern of the signal traces gets symmetrical. In addition, the ICPA is linearly polarized. The E_{ϕ} component dominates in the E-plane and the E_{θ} component in the H-plane. The

radiation level differences between E_ϕ and E_θ components in both planes are affected evidently by the alterations. For example, the larger differences can be observed in the broadside direction for the cases of the removal of the balls and the thinner top layer. This implies that the co-polarization radiation becomes stronger and the cross-polarization radiation becomes weaker. The efficiency and gain of the ICPA are slightly affected with respect to various alterations to the ICPA. The highest efficiency 74% occurs for the case of the removal of the solder balls and the lowest efficiency 70% occurs for the case of the thicker top layer. The reasons are because the removal of the solder balls reduces the conductor loss and the thicker top layer enhances the surface wave. Since the radiation patterns are similar, especially in the upper hemisphere, the highest efficiency yields the highest gain 4.9 dBi for the case of the removal of the solder balls and the lowest efficiency and a poor matching account for the lowest gain 4.6 dBi for the case of the thicker top layer.

IV. Conclusion

This paper has focused on the development of novel integrated circuit package antennas for highly integrated RF transceivers. A compact ICPA has been designed and fabricated in a CBGA package format for the first time. The effects of the different physical parts of the ICPA on the antenna performance have been investigated using the FDTD method. Results show that the ICPA achieved impedance bandwidth of 4.1% and radiation efficiency of 72%, and gain of 4.8 dBi at 5.715 GHz.

The inventive ICPA, except better performance than conventional dielectric chip antennas, enjoys economical advantage of mass production and automatic assembly and has potential benefit to the system-level board miniaturization and the system-level manufacturing facilitation. It is therefore anticipated that the results and design details on the ICPA presented here are useful and inspiring for engineers interested in antenna-package-chip codesign of novel wireless communications systems.

Acknowledgment

The author would like to thank Ms. J. J. Wong, Mr. C. C. Zhang, Mr. J. J. Liu, Mr. C. K. Sim, Mr. W. C. Sim, Ms. C. T. Sim, and Mr. S. K. Sin for their assistance in this work.

References

[1] H. Samavati, H. R. Rategh, and T. H. Lee, "A 5-GHz CMOS wireless LAN receiver front end," *IEEE J. Solid-State Circuits*, vol. 35, pp. 765–772, May 2000.

[2] K. Yamamoto, T. Heima, A. Furukawa, M. Ono, Y. Hashizume, H. Komurasaki, S. Maeda, H. Sato, and N. Kato, "A 2.4-GHz-band 1.8 V operation single-chip Si-CMOS T/R-MMIC front-end with a low insertion loss switch," *IEEE J. Solid-State Circuits*, vol. 36, pp. 1186–1197, Aug. 2001.

[3] R. G. Arnold, "RF IC and MCM-D codesign for wireless communication systems," in *Proc. IEEE Int. Workshop on Chip-Package Codesign*, 1998, pp. 53–58.

[4] S. Donnay, P. Pieters, K. Vaesen, W. Diels, P. Wambacq, W. D. Raedt, E. Beyne, M. Engels, and I. Bolsens, "Chip-package codesign of a low-power 5-GHz RF front end," *Proc. IEEE*, vol. 88, no. 10, pp. 1583–1597, 2000.

[5] Y. P. Zhang, T. K. C. Lo, and Y. Hwang, "A dielectric loaded miniature antenna for microcellular and personal communications," in *Proc. IEEE Int. AP-S Symp.*, 1995, pp. 1152–1155.

[6] H. Tanidokoro, N. Konishi, E. Hirose, Y. Shinokara, H. Arai, and N. Goto, "1-wavelength loop type dielectric chip antenna," in *Proc. IEEE Int. AP-S Symp.*, 1998, pp. 1950–1953.

[7] Y. Dakeya, T. Suesada, K. Asakura, N. Nakajima, and H. Mandai, "Chip multilayer antenna for 2.45 GHz-band application using LTCC technology," in *Digest IEEE Int. MTT-S Int. Symp.*, 2000, pp. 1693–1696.

[8] S. H. Sim, C. K. Kang, S. J. Yoon, Y. J. Yoon, and H. J. Kim, "Broadband multilayer ceramic chip antenna for handsets," *Electron. Lett.*, vol. 38, no. 5, pp. 205–207, 2002.

[9] W. Choi, S. Kwon, and B. Lee, "Ceramic chip antenna using meander conductor line," *Electron. Lett.*, vol. 37, no. 15, pp. 933–934, 2001.

[10] C. Y. Pan and T. S. Horng, "Miniaturized dielectric chip antenna in a C-shaped configuration with an array of shorting pins," in *Proceedings of APMC*, 2001, pp. 480–482.

[11] E. Tentzeris *et al.*, "Design of compact stacked-patch antennas on LTCC technology for wireless communication applications," in *Proc. IEEE Int. AP-S Symp.*, 2002, pp. 500–503.

[12] R. L. Li, G. Dejean, M. M. Tentzeris, J. Laskar, and J. Papapolymerou, "LTCC multilayer based CP patch antenna surrounded by a soft-and-hard surface for GPS applications," in *Proc. IEEE Int. AP-S Symp.*, 2003, pp. 651–654.

[13] *A One-Chip Design Solution for Bluetooth Wireless Applications*, 2001.

[14] *MTC60110 Radio Transceiver*, 2001.

[15] Y. P. Zhang, "Integration of microstrip patch antenna on ceramic ball grid array package," *Electron. Lett.*, vol. 38, no. 5, pp. 207–208, 2002.

[16] R. F. Drayton, R. M. Henderson, and L. P. B. Kathhi, "Monolithic packaging concepts for high isolation in circuits and antennas," *IEEE Trans. Microwave Theory Tech.*, vol. 46, pp. 900–906, July 1998.

[17] K. L. Virga and Y. Rahmat-Sammi, "Low-profile enhanced-bandwidth PIFA antennas for wireless communications packaging," *IEEE Trans. Microwave Theory Tech.*, vol. 45, pp. 1879–1888, Oct. 1997.

[18] D. Singh, C. Kalialakis, P. Gardner, and P. S. Hall, "Small H-shaped antennas for MMIC applications," *IEEE Trans. Antennas Propagat.*, vol. 48, pp. 1134–1141, July 2000.

[19] M. S. Tong, M. W. Yang, Y. C. Chen, and R. Mittra, "Finite-difference time-domain analysis of a stacked dual-frequency microstrip planar inverted-F antenna for mobile telephone handsets," *IEEE Trans. Antennas Propagat.*, vol. 49, pp. 367–376, Mar. 2001.

[20] Z. P. Liao, H. L. Wong, B. P. Yang, and Y. F. Yuan, "A transmitting boundary for transient wave analysis," *Scientia Sinica Series A*, vol. 27, no. 10, pp. 1063–1076, 1984.

[21] K. F. Lee and W. Chen, *Advances in Microstrip and Printed Antennas*. New York: Wiley, 1997.

[22] M. Zhang, Q. Chen, P. S. Hall, and V. F. Fusco, "Broadband microstrip patch antenna on micromachined silicon substrates," *Electron. Lett.*, vol. 34, no. 1, pp. 3–4, 1998.

Y. P. Zhang received the B.E. and M.E. degrees from Taiyuan Polytechnic Institute and Shanxi Mining Institute of Taiyuan University of Technology, Shanxi, China, in 1982 and 1987, respectively and the Ph.D. degree from the Chinese University of Hong Kong, Hong Kong, in 1995, all in electronic engineering.

From 1982 to 1984, he worked at Shanxi Electronic Industry Bureau, from 1990 to 1992, the University of Liverpool, Liverpool, U.K., and from 1996 to 1997, City University of Hong Kong. From 1987 to 1990, he taught at Shanxi Mining Institute and from 1997 to 1998, the University of Hong Kong. He was promoted to a Full Professor at Taiyuan University of Technology in 1996. He is now an Associate Professor of the School of Electrical and Electronic Engineering, Nanyang Technological University, Singapore. He has worked in the areas of propagation of radio waves, characterization of radio channels, miniaturization of antennas, and implementation of wireless communications systems. He is currently guiding a research group at the Integrated Systems Research Laboratory to develop radio technologies for inter- and intra-chip wireless interconnection, communications, and networking.

Prof. Zhang received the Sino-British Technical Collaboration Award in 1990 for his contribution to the advancement of subsurface radio science and technology. He also received the Best Paper Award from the Second International Symposium on Communication Systems, Networks, and Digital Signal Processing, 18–20th July 2000, Bournemouth, U.K. He is listed in *Marquis Who's Who in Science and Engineering* and *Cambridge IBC 2000 Outstanding Scientists of the 21st Century*. He serves on the Editorial Board of the *International Journal of RF and Microwave Computer-Aided Engineering* and as a Guest Editor of the Journal for the special issue *RF and Microwave Subsystem Modules for Wireless Communications*.